

A Novel Two-Station Seismic Method to Locate Glacier Calving

M. Jeffrey Mei¹ and David M. Holland²

¹Department of Physics, New York University Abu Dhabi

²Courant Institute of Mathematical Sciences, New York University

May 12, 2015

Abstract

A novel method of determining glacier calving location using hyperbolas from two local seismic stations is presented. The wave arrival time difference is used to define a locus of possible origins, which intersects uniquely with the calving front. This method is motivated by difficulties with traditional seismic location methods that fail due to the emergent nature of calving, which obscures the P and S-wave onsets, and the proximity of the seismometers, which combines body and surface waves into one arrival. A mix of tidal and seismic data and satellite imagery are used to confirm a list of calving events at Helheim Glacier from August 2013 to August 2014. In particular, two events in the week beginning August 11 2014 that were seen in person are used to calibrate the method, which is then applied to other calving events. An extension of this method with one more station would allow for triangulation location that would not depend on satellite or camera imagery.

can help narrow down the manual search in satellite and camera imagery for calving, but ultimately, locating events is still dependent on clear weather and well-lit conditions (O’Neel et al., 2007).

In particular, seismic (sound) and tsunami meter (water pressure data) are much more useful than simple camera or satellite imagery because seismic and tsunami meter arrays are not limited to daylight hours, are not affected by snow, and also provide quantitative data to help estimate the magnitude of calving events. Other seismic studies of calving have been done at the local/regional (<200km, e.g. Amundson et al. (2008), Amundson et al. (2012), O’Neel et al. (2007) as well as the teleseismic level (e.g. Walter et al. (2012), Chen et al. (2011)). Generally, teleseismic detections of calving are done via low-frequency surface waves (due to high-frequency wave attenuation) and local detections are done at some range of frequencies within 1-10 Hz.

1 Introduction

The calving of icebergs is a significant contributor to rising sea levels worldwide due to the massive volumes of ice involved that can suddenly be discharged into the sea. However, the lack of understanding of the physical and mathematical principles that cause these events means that it is difficult to forecast precisely the expected sea level rise in the near future (e.g. Pfeffer et al. (2008), Meier et al. (2007)). Calving glaciers can rapidly retreat in response to climate signals, and this can rapidly change the sea level (Meier and Post, 1987)). A better understanding of calving processes is vital to developing accurate predictions of sea level rise.

The lack of understanding of why and how calving events happen makes it hard to predict calving events and currently, detection methods require visual confirmation of the location. There have been few direct calving observations (e.g. Qamar (1988), Amundson et al. (2008)) and even fewer for which there exists complete seismic, tidal and satellite data. This is simply because calving events are somewhat intermittent, even if they also exhibit seasonality due to the seasonality of the mélange ice (Foga et al., 2014; Joughin et al., 2008), so monitoring equipment has to be deployed long-term in order to capture these events. Automated detection methods include measuring ratios of short-time-average (STA) and long-time-average (LTA) seismic signals, which

The seismic signals generated by glacial calving are believed to be caused either by capsizing icebergs striking the fjord bottom (Amundson et al., 2012; Tsai et al., 2008), or by sliding glaciers that speed up after calving (Tsai et al., 2008). Regardless of the cause, these seismic signals typically have emergent onsets with dominating frequencies around the order of 1-10 Hz (Richardson et al., 2010; O’Neel et al., 2007; Amundson et al., 2012).

The emergent signals means it is hard to accurately identify a P-wave onset time, let alone a S-wave onset time, which prevents traditional seismic location methods that involve taking the time difference between the P and S waves (Spence, 1980).

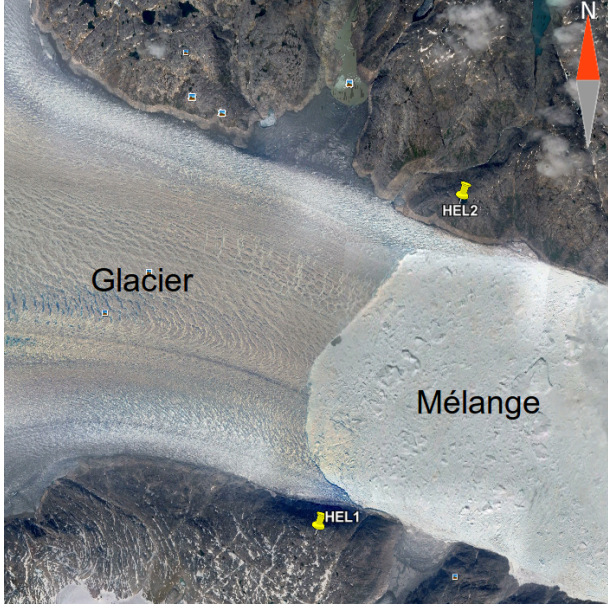


Figure 1: The two bedrock deployed seismometers. GPS coordinates for HEL1: $66^{\circ}19'45.6''\text{N}$ $38^{\circ}8'47.4''\text{E}$, HEL2: $66^{\circ}23'14.6''\text{N}$ $38^{\circ}5'54.5''\text{W}$. The calving front is clearly visible in between them. To the right of it is the mélange and Sermilik Fjord; to the left is Helheim Glacier.

Other typical methods that involve calculating backazimuths from a ratio of easting and northing amplitudes of P waves from a broadband seismic station (e.g. Jurkevics (1988)) also fail due to the proximity of the station and the high speed of the sound waves (4 km/s through ice) which renders all the wave arrivals near-simultaneous.

On August 12 and August 13 2014, calving events were seen with the naked eye at Helheim Glacier. These events, referred to as Calving Event I and Calving Event II (CE-I, CE-II) respectively, are helpful to calibrate the hyperbolic method, which can then be applied to other unseen events at Helheim Glacier.

2 Identifying Calving

Two broadband seismometers with sampling rate 40 Hz were deployed around the mouth of Helheim Glacier, situated 6.88 km apart.

Our calving signals match those of Amundson et al. (2012) very well, with an emergent onset and a power spectrum dominating in the 1-10Hz range (see Figure 2). In contrast, teleseismic events from regional earthquakes have much lower frequency signals, below 0.1 Hz (see Figure 3). We filter for 2-18 Hz based off these spectrograms in order to maximize the signal-to-noise ratio for our hyperbolic location

method. This is likely to filter out surface waves as these have maximum power in the 0.01-0.5 Hz range (Montalbetti and Kanasewich, 1970), though the hyperbolic method does not depend on the wave type so this is not an issue.

3 Location Methods and Results

3.1 Backazimuth method

A standard method for locating earthquakes is based off calculating the backazimuth via a ratio of easting and northing amplitudes, following single-station methods from seismology (e.g. Alessandrini et al. (1994)). This method relies on the speed difference between P and S waves, such that the P wave, which is linearly polarized collinear with the source-to-receiver direction, arrives significantly faster than the S wave. In our data, the surface (Love and Rayleigh) waves arrive almost simultaneously with the P wave and so the azimuthal method does not work. Linear fits to a 2D particle plot showing the ground motion of the East vs North channels are shown in Figure 4 for a teleseismic event, and in Figure 5 for a calving event. Our teleseismic event, which occurred in Atka, Alaska in the United States was sufficiently far to have a P wave arrival before the other seismic waves (moreover, the ocean between Atka and Helheim also removes shear waves). This makes the backazimuth method effective for teleseismic events, but not for calving events.

3.1.1 2D method

The two particle plots in Figure 4 look very similar, as expected for a teleseismic event where the signal is sufficiently far, such that HEL1 and HEL2 are essentially the same receiver relative to the Atka epicenter. In contrast, the calving events, which take place between HEL1 and HEL2, should produce particle plots of P-waves that have opposing gradients (such that the one has positive gradient and the other has a negative gradient, so the two lines converge). In Figure 5, we can see that this indeed the case, however; the fit for HEL1 on the left is somewhat dubious and should really be considered a null fit. Moreover, the azimuth corresponding to the fit for HEL2 points into the mélange, which is unphysical. The strength of that fit, however, suggests that the line of best fit is not representing the P-wave alone, but perhaps a mix of P and surface waves, with the surface waves potentially dominating the P-wave. It is possible that most of the

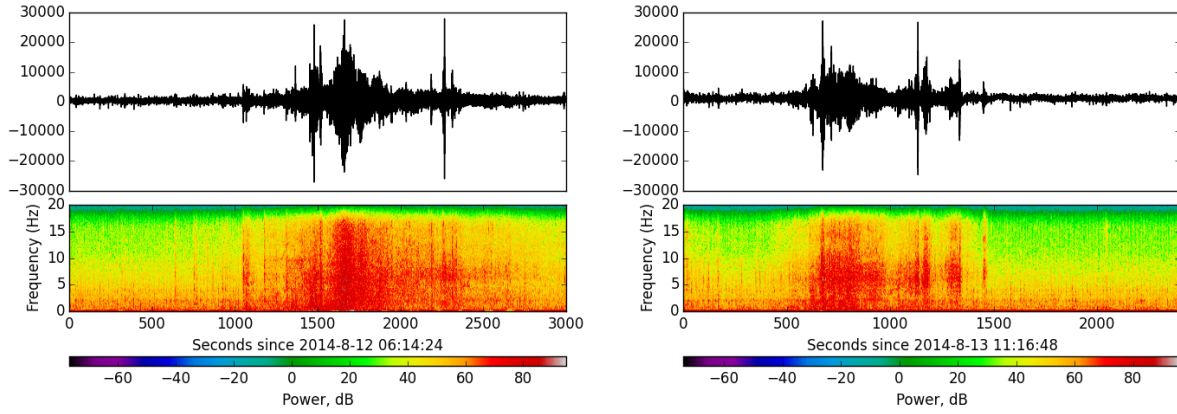


Figure 2: Spectrograms for CE-I, the calving event of August 12 (left), and of CE-II on August 13 (right) in 2014. The y-axis of the top panels shows counts, a dimensionless quantity, from the East channel of the seismometers.

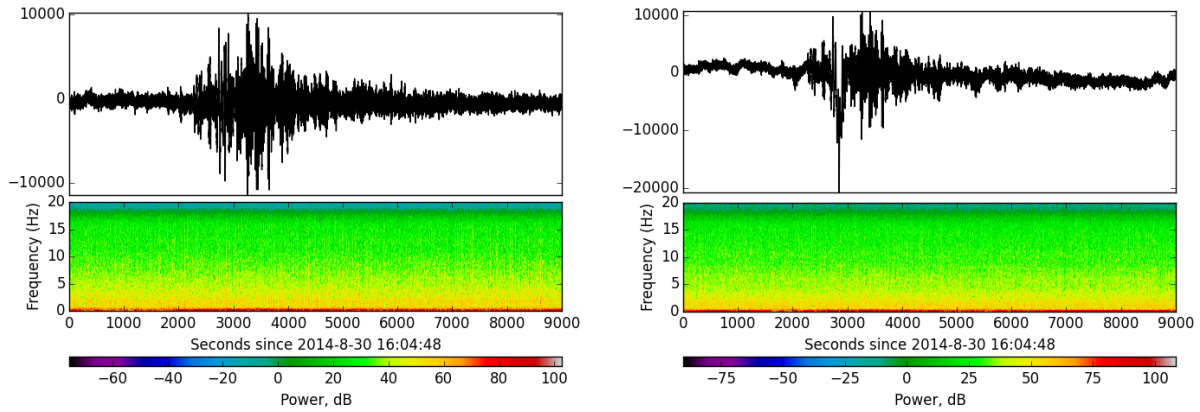


Figure 3: Spectrograms for the teleseismic event from Atka, AK, United States discussed in Figure 4 from HEL1 (L) and HEL2 (R), showing the different frequency distribution when compared to calving events as well as the similarity in signals relative to each other.

energy comes from Love waves, in the case of low-to-moderate impedance contrast $Z = \rho_i/\rho_r \times v_i/v_r$ for densities of ice (ρ_i) and rock (ρ_r) and compressional wave speeds in ice (v_i) and rock (v_r), which is the case here where $Z < 1$ (Bonnefoy-Claudet et al., 2008).

The failure of the 2D azimuthal method due to the concurrent arrivals of the differently-polarized P, S and surface waves motivates an investigation into the 3D particle plots in order to see if surface waves are dominating body waves or vice versa.

3.1.2 3D method

The 3D particle plots reveal the characteristic elliptical shape of the Rayleigh wave. This can be strengthened by bandpass filtering (Butterworth, two-pole and zero-phased) between 0.01 and 0.05 Hz, which are empirically determined to maximize the surface

waves. This is seen in Figure 6 and 7. However, the fitted plane in Figure 8, which aligns in theory with the Rayleigh wave, is slightly off-axis. A theoretical Rayleigh wave is aligned with the vertical direction, and so this deviation is possibly due to shearing from the Love wave, which would have arrived concurrently. Assuming that the Love wave only affects motion in the x-y direction, this means that the projection onto the x-y plane of the normal vector characteristic of the fitted plane would be the direction of the Love wave (as it must be perpendicular to the Rayleigh wave). This fit, while strong, as seen in Figure 8, is unphysical: the normal vector corresponds to an arctangent of -67° , which is in theory perpendicular to the Rayleigh wave, so $+23^\circ$. However, from HEL1, this points into the mélange - and we know that CE-II happened at a bearing of approximately -45° from HEL1. This is closer in fit to the supposed Love wave and it seems like the Love and

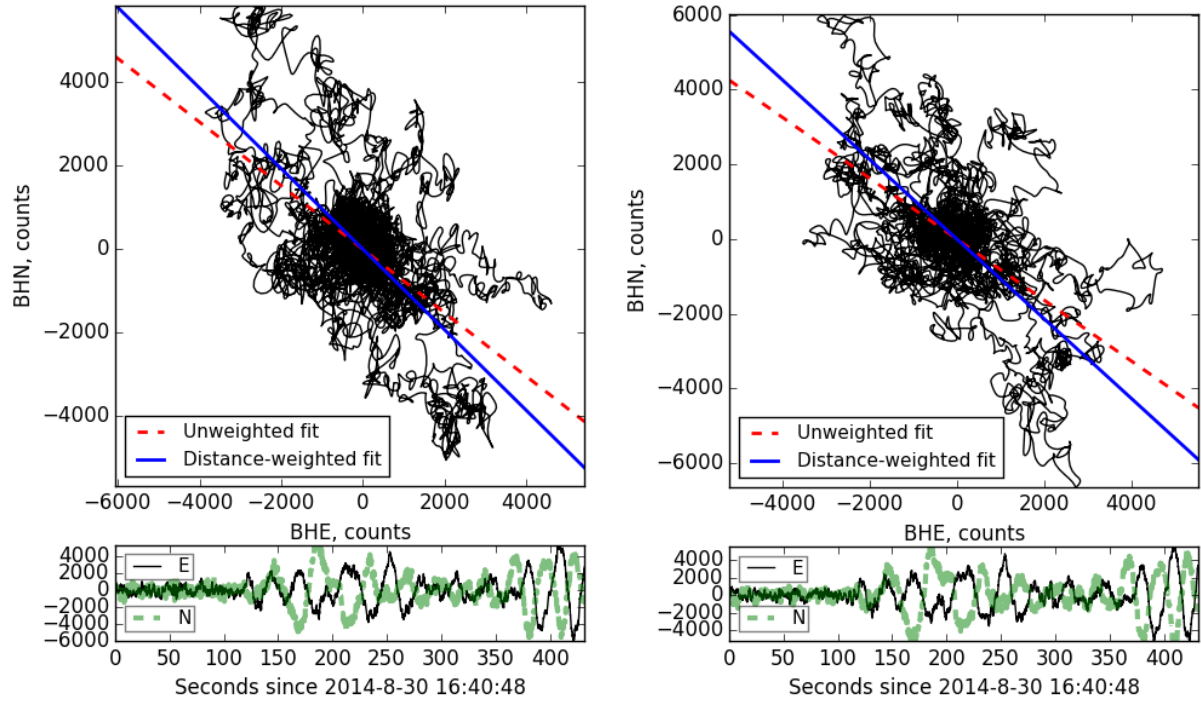


Figure 4: Particle plots for a teleseismic event near Atka, AS, United States, as seen on HEL1 (L) and HEL2 (R), on the Broadband High-Gain North (BHN) and Broadband High-Gain East (BHE) channels. These have been filtered between 0.0001 Hz and 0.5 Hz to emphasize the signal.

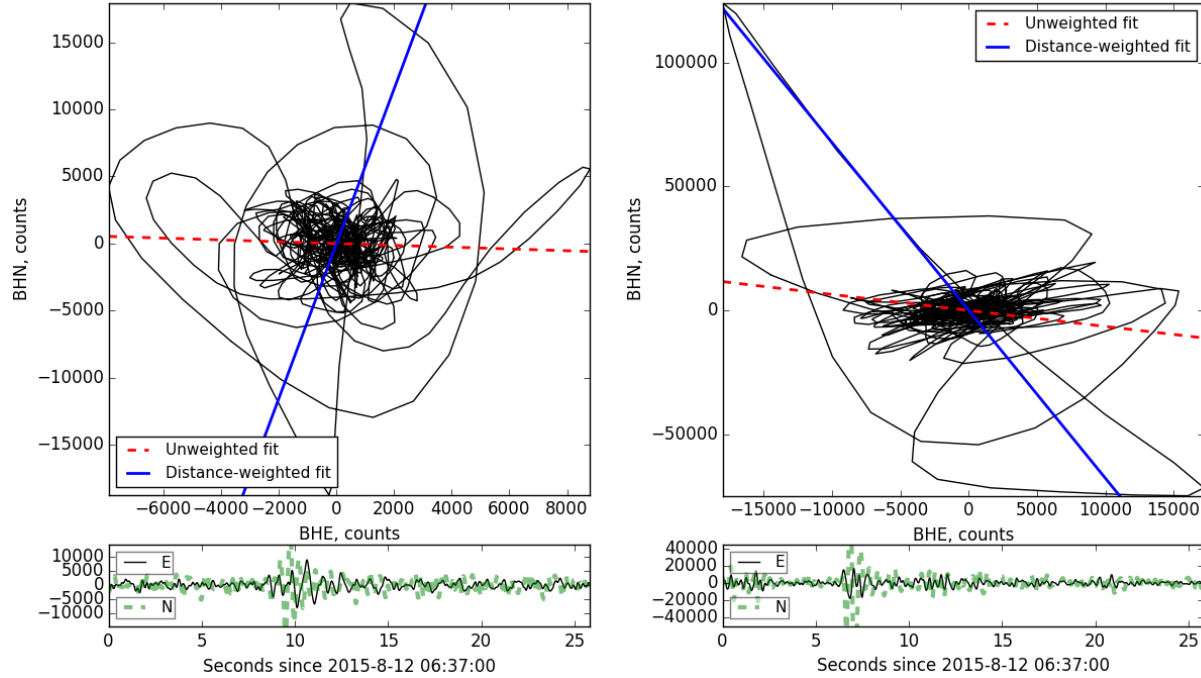


Figure 5: Particle plots for CE-I, as seen on HEL1 (L) and HEL2 (R). These have been filtered between 0.01 and 0.5 Hz to emphasize the signal. Note the several seconds of lag between the wave arrivals at HEL1 with respect to HEL2.

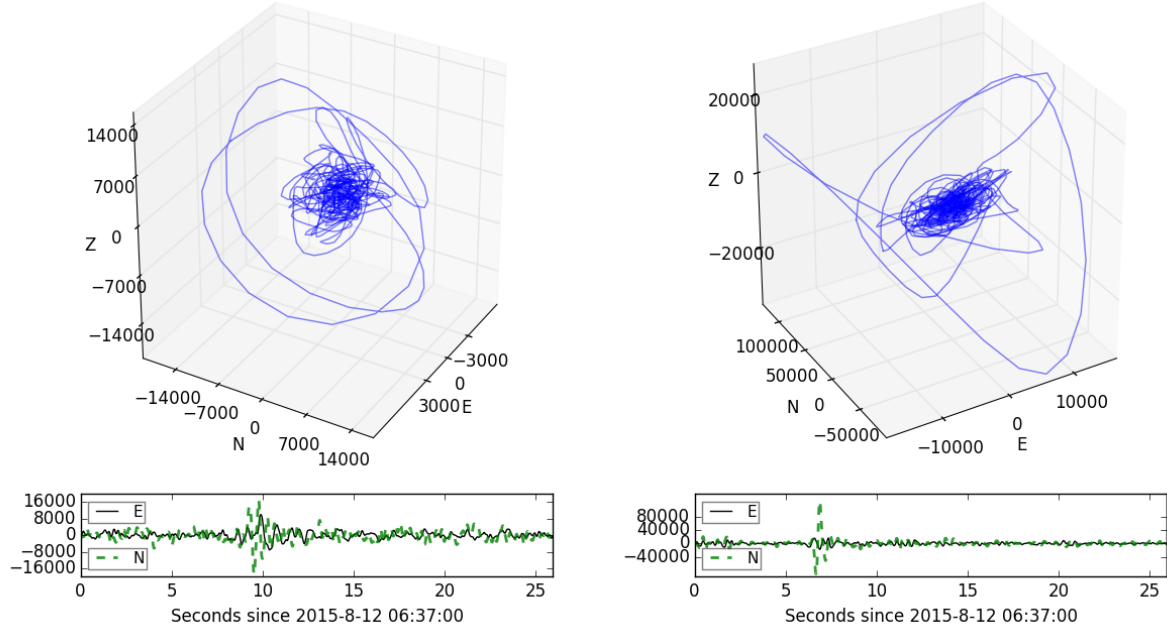


Figure 6: 3D particle plots for CE-I in Helheim as seen on HEL1 (L) and HEL2 (R). These have been filtered between 0.01 and 0.5 Hz to emphasize the signal. Note the 2.28 s lag between the wave arrivals at HEL1 with respect to HEL2 and the clear presence of the elliptical Rayleigh waves in the signals.

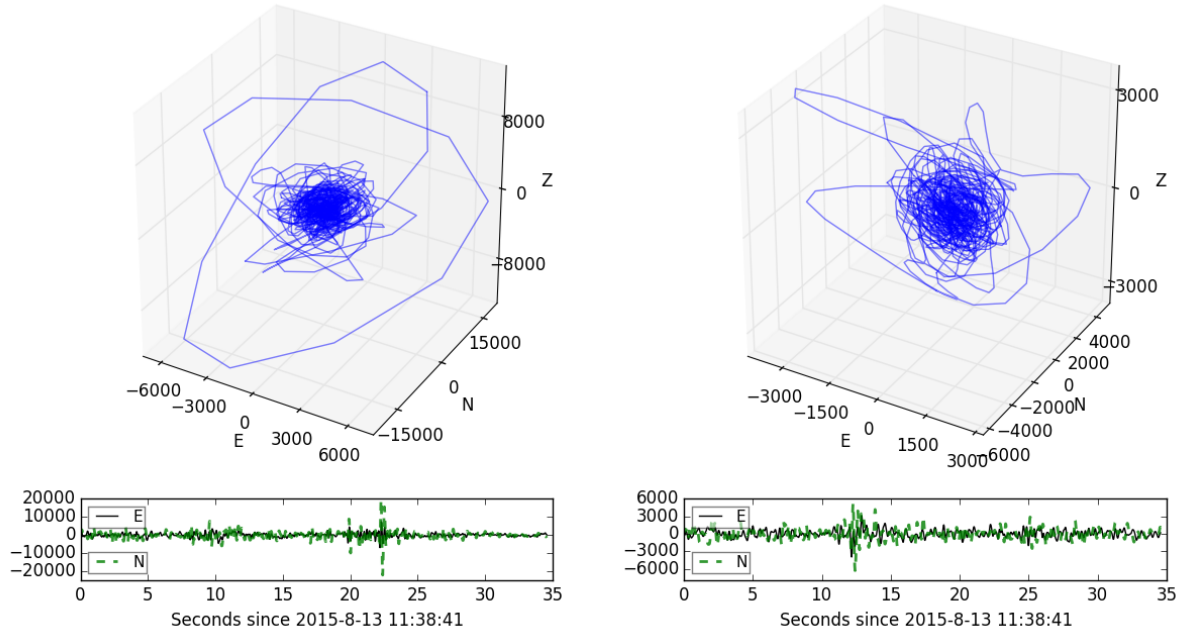


Figure 7: 3D particle plots for CE-II in Helheim as seen on HEL1 (L) and HEL2 (R). There is a 2.65 s lag between the wave arrivals at HEL2 with respect to HEL1. Note the clarity of the elliptical Rayleigh wave in the HEL1 signal relative to the noisier HEL2 signal.

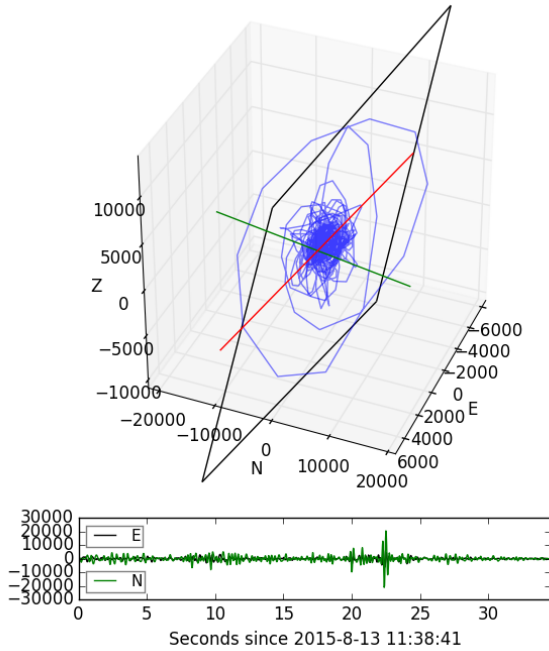


Figure 8: 3D particle plots for CE-II as seen from HEL2, with the plane fitted to the Rayleigh wave, the normal vector corresponding to the plane (green) and the projection of the normal vector onto the East-North plane (red).

Rayleigh waves have been switched around. One possible explanation is that the glacier surface is slightly anisotropic: in this case, the Rayleigh waves would not necessarily align up with the P-wave polarization (Smith and Dahlen, 1973). It is likely that the mix of different wave phases has created some kind of sheared Rayleigh wave such that it no longer aligns with the z-axis. The implausibility of this fit motivates the creation of another method, one that does not depend on being able to distinguish the different wave types: this is the motivation for the Hyperbolic Method.

3.2 Hyperbolic Method

If a calving event happened at a point on the perpendicular bisector of HEL1 and HEL2, then the equal path length from the event to the seismometers would mean that we would expect that the two seismometers would register the event at the exactly the same time. Similarly, if the event happened closer to HEL1, it would arrive slightly faster there and the locus of possible calving locations would be the set of all points whose distance from HEL1 is shorter than HEL2 by a fixed length, $2a$, which would be the product of the speed of the waves

through the glacier and the time lag in signal arrival. As a hyperbola can be defined as the set of all points with a constant path difference (equal to $2a$, for a hyperbola of equation $x^2/a^2 - y^2/b^2 = 1$: see Figure 9) when measured from the two foci, we may use the time lag of the signal arrivals at the two seismometers (which become our foci) to determine the path difference of the signals, and from this deduce the loci of possible signal sources. One of the arms (in Figure 9, either the left curve or the right curve) of the hyperbola may always be eliminated, as we can see which seismometer the event was closer to from seeing which station has the first signal onset.

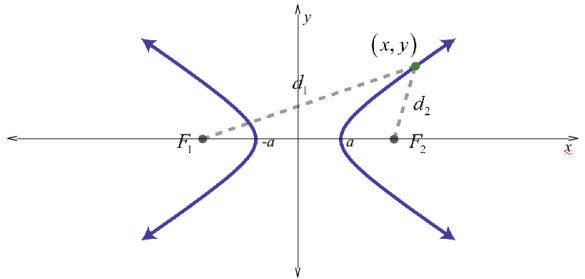


Figure 9: An example of a hyperbola, with foci at F_1 and F_2 with constant path difference $|d_2 - d_1| = 2a$.

This method involves evaluating the time lag between the signal arrival times at the two seismometers, and obtaining the speed of seismic waves (unknown if P or Rayleigh/Love) through the glacier. This assumes that the wave travels the same speed in both directions, which is reasonable as the medium is the same.

The only unknown here is the speed of the seismic wave through the glacier. A natural upper bound for the speed is the speed of sound (or a P-wave) through ice, which is 3.8 km/s (Bentley, 1972). Given our signal delay times and the length of the calving front, this is physically impossible as a width of 6.9 km would only permit a maximum time difference of 1.8 s, which our measurements exceed. In fact, given a maximum signal time difference of 3 s, the upper bound for velocities obtained by assuming events happened right at the seismometer is 2.3 km/s. As our two calving events were visually confirmed to have taken place at some distance away from the seismometers, the seismic wave speed through Helheim is likely significantly lower than this. We also note that our signal is dominated by surface waves, which have higher amplitude than body waves, and that the speed of a S wave (which is faster than a surface wave) in ice is 1.96 km/s (Bentley, 1972; Kohnen, 1974).

The geometry of glaciers may affect seismic

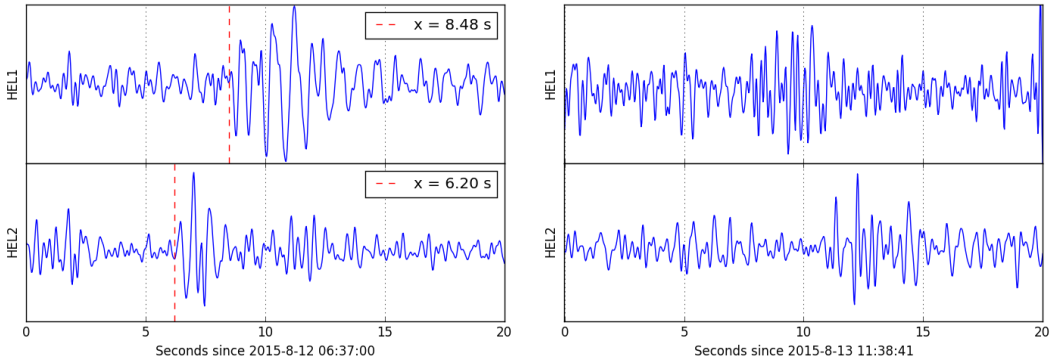


Figure 10: Signals for CE-I (L) and CE-II (R) at HEL1 and HEL2. For CE-I, the signal lag is very easy to measure, while for CE-II, the exact lag is not clear even though the lag is visibly present.

wave speeds, slowing it down due to their porosity (Kohnen, 1974). The S-wave velocity of a meters-thick ice stream in Antarctica was worked out as 0.15 km/s, corresponding to a porosity of 40% (Blankenship et al., 1986). It is unclear what porosity Helheim Glacier is, though the density of glaciers, around 850 kg/m³, is higher than the 550 kg/m³ of ice of 40% porosity (Vasil'chuk and Vasil'chuk, 2003) and so 0.15 km/s would be a lower bound. For our purposes, we use a variety of speeds to plot our hyperbolae, namely 0.2 km/s, 0.7 km/s, 1.2 km/s, 1.7 km/s.

4 Discussion

The novel hyperbolic method described in this paper offers a powerful alternative to traditional seismic location techniques, which are more suited for regional seismic arrays that can distinguish between the different seismic wave types (e.g. O’Neil et al. (2007)). Moreover, these distant arrays do not give the kind of precision of calving location that local arrays would have, as small errors on the azimuth translate to a large area of uncertainty on the glacier surface. The hyperbolic method takes advantage of the stations’ proximity to calving events and does not require separating out the different wave phases, thus solving the P-wave identification problem that hampered locating techniques from Amundson et al. (2008) and Richardson et al. (2010).

The method also offers advantages over traditional calving detection methods, which require the use of a local camera and/or satellite data to visually confirm that calving took place. As seen in (Amundson et al., 2012), calving also generates a characteristic seismic signal. In Figures 2 and 3, we directly compare teleseism with calving and note that teleseism does not have any energy above 5 Hz or so, and have most of their energy <1 Hz, likely because

higher frequency signals are severely attenuated by the time they reach the seismometers. This means that seismometers could be used to monitor glaciers and quickly identify calving when power in the 2–18 Hz range exceeds some particular value above the ambient noise. Importantly, this monitoring could take place during night and also cloudy days, thus replacing satellite and camera imagery as the primary method for identifying calving.

One issue is attempting to constrain the seismic wave speed within glaciers. O’Neil et al. (2007) used a P-wave speed of 3.25 km/s, which is slightly lower than a typical speed, e.g. 3.8 km/s in Robinson (1968). This is due to the fractured and water-saturated nature of the glacial ice. Similarly, in our case, we do not know what the seismic wave speed is. This is easy to test and in subsequent expeditions to Helheim glacier, we hope to detonate explosives near one seismometer and measure the time taken for the seismic waves to reach the other seismometer and to use this speed. A speed of 3 km/s seems impossible for our data, as a time lag of 2.6 seconds at 3 km/s would mean a path difference of more than 7 km, i.e. more than the distance between the two seismometers, which is not possible under our model of uniform wave propagation in all directions. As we also see a strong presence of elliptical Rayleigh waves, it is likely that the waves that we use for our hyperbolic method are surface waves, which travel markedly slower than P-waves, with a lower bound of 0.15 km/s from porous sea ice in Blankenship et al. (1986).

The calculation method we have used ignores the presence of the rock, as the proximity of the seismometers to the glacier makes the time the wave spends travelling across rock negligible compared to the time spent on the glacier. However, our method does not take into account the refraction at the ice-rock interface. Again, due to the ice dominating the

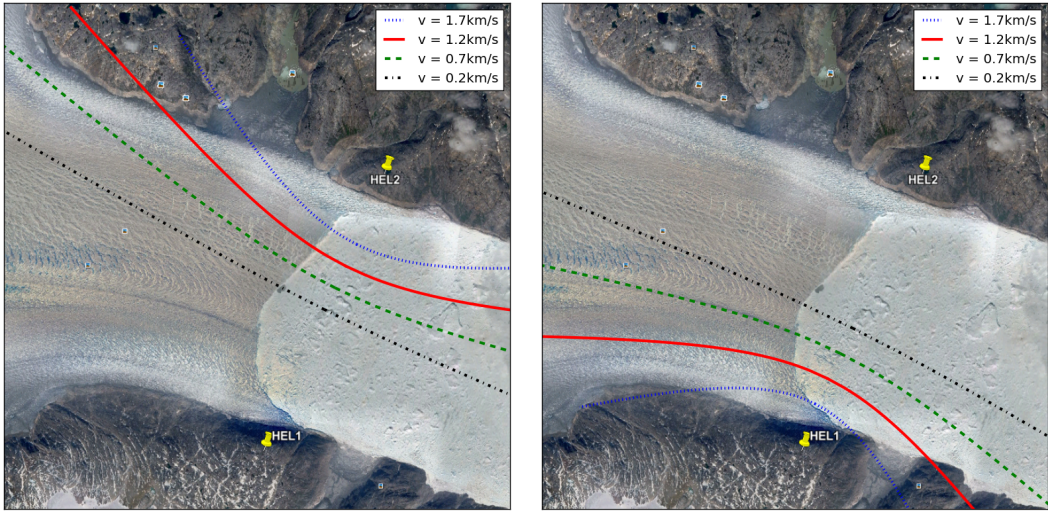


Figure 11: Hyperbolic loci for CE-I (L) and CE-II (R) for a variety of wave propagation speeds in the glacier. The background satellite image is from July 2014, i.e. 6 weeks before these events occurred, is an only approximately accurate depiction of the calving front for these events.

wave path from the source to the seismometers, we may assume that the refraction has a negligible affect on the azimuthal measurement. It is also possible that the seismic wave travels along the bottom of the glacier at the rock-ice interface, and then comes up the rock surrounding the glaciers. While we cannot prove this to be impossible, the higher speed of sound through rock would give much larger path differences corresponding to event locations much closer to the seismometers, which was not observed for CE-I and CE-II.

Similarly, our method does not take into account the height of seismometers relative to the glacier. As

the seismometers are 300 m or so above the glacier, this means that a linearly polarized P-wave, instead of just having East and North components, will also have some Z component. However, our attempts at azimuth calculation using a bandpass filter of 0.01-0.05 Hz, give approximate surface wave wavelengths of 20-100 km, using $v_{sound} = 1$ km/s through the glacier. This is much longer than the height difference of 0.200 km, and so it is unlikely to affect the Z-channel by much.

A further extension of this method is in progress, with two additional seismometers deployed, bringing the total to four. Just three seismometers would be

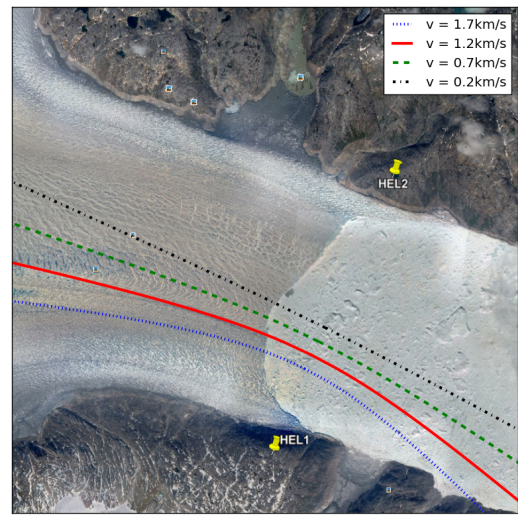
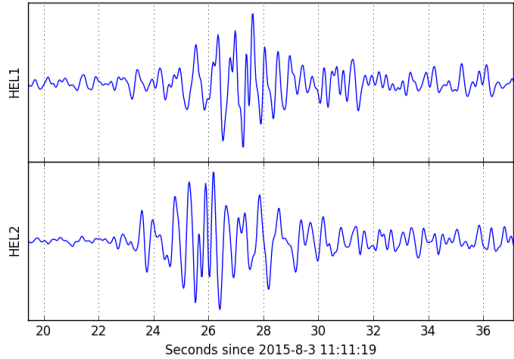


Figure 12: A third calving event from August 3, 2014, with a clear signal time lag of 1.8 s between the two stations. Again, this satellite imagery is slightly outdated, from a month before the calving event.

enough to generate 3 hyperbolae, which would ostensibly intersect at the signal source and allow for triangulation even without knowing the difference in onset time of P and S waves. It may also be possible to capture the depth of the initial shaking, if a three-dimensional hyperboloid is used instead of a two-dimensional hyperbola.

Our results show that there are ways to get around the emergent P-wave problem for glacial calving, which have characteristic power spectra, via the development of a hyperbolic method that simply measures the time delay in the signal arrival times at two seismometers. With three seismometers, triangulation becomes possible, and calving events can be automatically detected and located, even without satellite or camera imagery. This method can be extended to other glaciers by measuring their characteristic seismic wave speed empirically to calibrate this method. An automated calving detector and locator will dramatically increase the number of calving events that can be studied, in order to better understand the dynamics of calving.

Acknowledgements

The fieldwork necessary to collect this seismic data was made possible by the Center for Global Sea Level Change, grant G1204 of the NYU Abu Dhabi Research Institute and the Undergraduate Research Fund at NYU Abu Dhabi. The authors would also like to thank Irena Vankova for her catalogue of calving events from combining tsunami data and satellite imagery of Helheim.

References

- B. Alessandrini, M. Cattaneo, M. Demartin, M. Gasperini, and V. Lanza. A simple P-wave polarization analysis: Its application to earthquake location. *Annals of Geophysics*, 37(5), 1994.
- J. Amundson, M. Truffer, M. Lüthi, M. Fahnestock, M. West, and R. Motyka. Glacier, fjord, and seismic response to recent large calving events, Jakobshavn Isbræ, Greenland. *Geophysical Research Letters*, 35(22), 2008.
- J. M. Amundson, J. F. Clinton, M. Fahnestock, M. Truffer, M. P. Lüthi, and R. J. Motyka. Observing calving-generated ocean waves with coastal broadband seismometers, Jakobshavn Isbræ, Greenland. *Annals of Glaciology*, 53(60):79–84, 2012.
- C. R. Bentley. Seismic-wave velocities in anisotropic ice: A comparison of measured and calculated values in and around the deep drill hole at Byrd Station, Antarctica. *Journal of Geophysical Research*, 77(23):4406–4420, 1972.
- D. Blankenship, C. Bentley, S. Rooney, and R. Alley. Seismic measurements reveal a saturated porous layer beneath an active Antarctic ice stream. *Nature*, 322:54–57, 1986.
- S. Bonnefoy-Claudet, A. Köhler, C. Cornou, M. Wathelet, and P.-Y. Bard. Effects of Love waves on microtremor H/V ratio. *Bulletin of the Seismological Society of America*, 98(1):288–300, 2008.
- X. Chen, P. Shearer, F. Walter, and H. Fricker. Seventeen Antarctic seismic events detected by global surface waves and a possible link to calving events from satellite images. *Journal of Geophysical Research: Solid Earth (1978–2012)*, 116(B6), 2011.
- S. Foga, L. A. Stearns, and C. van der Veen. Application of satellite remote sensing techniques to quantify terminus and ice mélange behavior at Helheim Glacier, East Greenland. *Marine Technology Society Journal*, 48(5):81–91, 2014.
- I. Joughin, I. Howat, R. B. Alley, G. Ekstrom, M. Fahnestock, T. Moon, M. Nettles, M. Truffer, and V. C. Tsai. Ice-front variation and tide-water behavior on Helheim and Kangerdlugssuaq Glaciers, Greenland. *Journal of Geophysical Research: Earth Surface (2003–2012)*, 113(F1), 2008.
- A. Jurkevics. Polarization analysis of three-component array data. *Bulletin of the Seismological Society of America*, 78(5):1725–1743, 1988.
- H. Kohnen. The temperature dependence of seismic waves in ice. *J. Glaciol*, 13(67):144–147, 1974.
- M. Meier and A. Post. Fast tidewater glaciers. *Journal of Geophysical Research: Solid Earth (1978–2012)*, 92(B9):9051–9058, 1987.
- M. F. Meier, M. B. Dyurgerov, U. K. Rick, S. O’Neil, W. T. Pfeffer, R. S. Anderson, S. P. Anderson, and A. F. Glazovsky. Glaciers dominate eustatic sea-level rise in the 21st century. *Science*, 317(5841):1064–1067, 2007.
- J. F. Montalbetti and E. R. Kanasewich. Enhancement of teleseismic body phases with a polarization filter. *Geophysical Journal International*, 21(2):119–129, 1970.
- S. O’Neil, H. Marshall, D. McNamara, and W. Pfeffer. Seismic detection and analysis of icequakes at Columbia Glacier, Alaska. *Journal of Geophysical Research: Earth Surface (2003–2012)*, 112(F3), 2007.

W. T. Pfeffer, J. Harper, and S. O’Neel. Kinematic

constraints on glacier contributions to 21st-century sea-level rise. *Science*, 321(5894):1340–1343, 2008.

A. Qamar. Calving icebergs: A source of low-frequency seismic signals from Columbia Glacier, Alaska. *Journal of Geophysical Research: Solid Earth (1978–2012)*, 93(B6):6615–6623, 1988.

J. P. Richardson, G. P. Waite, K. A. FitzGerald, and W. D. Pennington. Characteristics of seismic and acoustic signals produced by calving, Bering Glacier, Alaska. *Geophysical Research Letters*, 37 (3), 2010.

E. S. Robinson. Seismic wave propagation on a heterogeneous polar ice sheet. *Journal of Geophysical Research*, 73(2):739–753, 1968.

M. L. Smith and F. Dahlen. The azimuthal dependence of Love and Rayleigh wave propagation in a slightly anisotropic medium. *Journal of Geophysical Research*, 78(17):3321–3333, 1973.

W. Spence. Relative epicenter determination using P-wave arrival-time differences. *Bulletin of the Seismological Society of America*, 70(1):171–183, 1980.

V. C. Tsai, J. R. Rice, and M. Fahnestock. Possible mechanisms for glacial earthquakes. *Journal of Geophysical Research: Earth Surface (2003–2012)*, 113(F3), 2008.

Y. K. Vasil’chuk and A. K. Vasil’chuk. *Types and Properties of Water*, volume 1-2. Encyclopedia of Life Support Systems, 2003.

F. Walter, J. M. Amundson, S. O’Neel, M. Truffer, M. Fahnestock, and H. A. Fricker. Analysis of low-frequency seismic signals generated during a multiple-iceberg calving event at Jakobshavn Isbræ, Greenland. *Journal of Geophysical Research: Earth Surface (2003–2012)*, 117(F1), 2012.